Electrochemistry
The Electrochemical Society of Japan
Received: January 17, 2024
Accepted: February 1, 2024
Published online: February 3, 2024
Issued: April 1, 2024
https://doi.org/10.5796/electrochemistry.24-69015
https://doi.org/10.50892/data.electrochemistry.25132577
Communication
Electrochemistry, **92(4)**, 043010 (2024)

The 69th special feature "Frontiers of Molten Salts and Ionic Liquids"

Electrochemical Characteristics of Lithium-Air Secondary Battery Using Amide-Based Ionic Liquids†

OPEN ACCESS

Koichi UI,[a,*,§] Sota NAKAMURA,[a,§§] Yushi SATO,[b] Tatsuya TAKEGUCHI,[a,§] and Masayuki ITAGAKI[c,d,§]

[a] *Graduate School of Arts and Science, Iwate University, 4-3-5 Ueda, Morioka, Iwate 020-8551, Japan*
[b] *Graduate School of Engineering, Iwate University, 4-3-5 Ueda, Morioka, Iwate 020-8551, Japan*
[c] *Department of Pure and Applied Chemistry, Faculty of Science and Technology, Tokyo University of Science, 2641 Yamazaki, Noda, Chiba 278-8510, Japan*
[d] *Research Institute for Science and Technology, Tokyo University of Science, Noda, Chiba 278-8510, Japan*

* *Corresponding author: kui@iwate-u.ac.jp*

ABSTRACT

We fabricated lithium-air secondary batteries (LABs) employing amide-based ionic liquids (ILs) as electrolytes and evaluated their electrochemical characteristics. Lithium bis(trifluoromethanesulfonyl)-amide (Li-TFSA) was employed as the lithium salt, *N*-methyl-*N*-propyl-pyrrolidinium-TFSA (Py_{13} system) with a cyclic aliphatic cation in the ILs, and *N*, *N*-diethyl-*N*-methyl-*N*-(2-methoxyethyl)ammonium-TFSA (DEME system) with an acyclic aliphatic cation. The constant-current discharge-charge tests with the capacity controlled at 200 mAh $(g\text{-carbon})^{-1}$ showed that the overvoltage of the LABs using the Py_{13} system was lower than those of LABs using the DEME system and the organic solvent-based system electrolyte. The cycling performance of the DEME system rapidly decreased at the 74th cycle, while the Py_{13} system showed 200 mAh $(g\text{-carbon})^{-1}$ up to the 100th cycle, indicating a high stability. Electrochemical impedance measurements showed that the LABs using the Py_{13} system had the lowest interfacial resistance after the 1st charge. These results indicated that the use of the Py_{13} system with a relatively high electrical conductivity and low viscosity as the electrolyte would stabilize the cycling performance of the LABs.

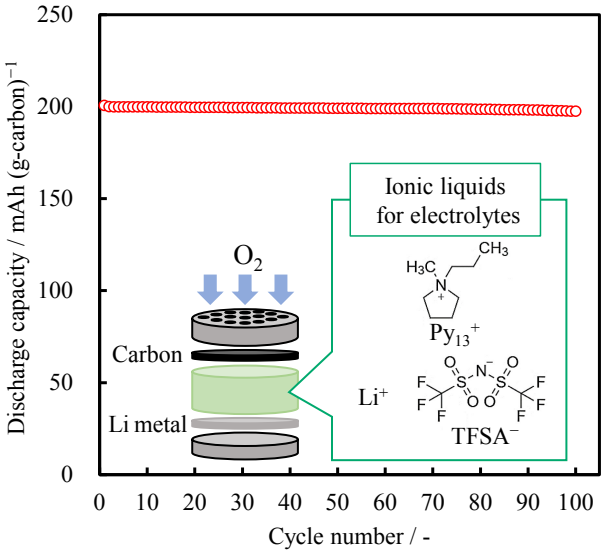

Keywords : Ionic Liquid, Lithium-air Secondary Battery, Air-electrode, Interfacial Behavior

1. Introduction

Lithium-air secondary batteries (LABs) have a high theoretical energy density (3458 Wh $(kg\text{-}Li_2O_2)^{-1}$)[1] and are expected to be the high-capacity next-generation secondary batteries. Recently, 500 Wh kg^{-1} class LABs, which greatly exceed the gravimetric energy density (300 Wh kg^{-1}) of current Li-ion batteries (LIBs), have been developed, and the discharge-charge reactions at room temperature have been reported.[2] However, there are several problems such as difficulty in the decomposition of the discharge products, the degradation of the air-electrode due to the discharge-charge reaction, the electrolyte volatilization, and the decomposition of the electrolyte due to the superoxide from the reaction intermediates,[3] which makes the discharge-charge reactions difficult for long cycling. In addition, the short-circuiting of the batteries due to the deposition of lithium (Li) dendrites on the Li negative electrode is also recognized as a major problem that threatens the battery safety.[4]

The electrolyte is one of the important factors affecting the discharge-charge characteristics of LABs. Currently, the organic solvent widely used in the LAB research is tetraethylene glycol dimethyl ether (tetraglyme, G4). The electrolytes using G4 as a solvent satisfy these conditions and have been widely used in obtaining basic knowledge about the LABs.[5,6] The effects of the Li salt type and O_2 gas on the precipitation and dissolution of Li were investigated using G4 as a solvent.[7] However, further basic research regarding the electrolytes has been conducted because many of them have poor battery characteristics. For example, it has recently been reported that the amide-based electrolytes exhibit a good cycling performance.[8] On the other hand, one of the attractions of non-volatile ionic liquids (ILs) is that they exhibit various physical

†The contents include the author's poster presentation P16 at the 2023 Joint Symposium on Molten Salts.
§ECSJ Active Member
§§ECSJ Student Member
K. Ui orcid.org/0000-0003-0754-1574
T. Takeguchi orcid.org/0000-0002-8520-3557

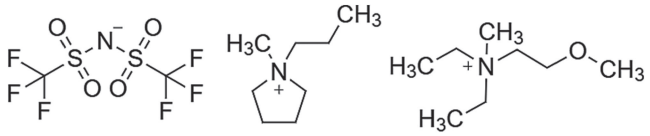

(a) $TFSA^-$(FW: 263.1) (b) Py_{13}^+(FW: 128.2) (c) $DEME^+$(FW: 146.3)

Figure 1. Structural formulas of aliphatic cations and the $TFSA^-$ anion.

properties depending on the combination of the cationic and anionic species. Structural changes in the cationic species, especially the introduction of functional groups, lead to various changes in the physical and electrochemical properties. For example, it has been reported that the introduction of ether into the side chain of an alkyl ring improves the ionic conductivity.[9] Additionally, the charge distributions of bis(trifluoromethanesulfonyl)amide (TFSA, Fig. 1a) and bis(fluorosulfonyl)amide (FSA) anions are delocalized. Hence, they are often used as a counter anion to facilitate the formation of ILs with a low viscosity.[10]

The effect of the structure of the cationic species of the ILs consisting of lithium bis(trifluoromethanesulfonyl)amide (Li-TFSA) as the lithium salt and $TFSA^-$ anion as the anion on the discharge-charge characteristics of the LABs has been reported. Compared to *N*-butyl-*N*-propylpyrrolidinium (Py_{14})-TFSA, the LABs using *N*-methyl-*N*-propylpyrrolidinium (Py_{13}, Fig. 1b)-TFSA as the electrolyte exhibited a better discharge-charge efficiency and cycling performance.[11] This is due to the short alkyl chain length of the side chain of the Py_{13}^+ cation, resulting in a high ionic conductivity. Compared to the cyclic *N*-methyl-*N*-propylpiperidinium (PP_{13})-TFSA, the initial discharge-charge characteristics of the LABs using the ether-introduced acyclic *N*, *N*-diethyl-*N*-methyl-*N*-(2-methoxyethyl) ammonium (DEME, Fig. 1c)-TFSA as the electrolyte was better.[12] This is due to the large size of the alkyl ring of the PP_{13}^+ cation and the relatively large formula amount. Additionally, LABs using DEME-TFSA as the electrolyte were able to achieve eight cycles at the discharge capacity limit of 100 mAh cm^{-2}.[13] As already mentioned, the battery characteristics of the LABs using Li-TFSA as the lithium salt, $TFSA^-$ anion as the anion, and an aliphatic cation have been reported, but the optimal combination of the cationic and anionic species has not yet been clarified. In addition, the relation between the ionic species constituting ILs and the interfacial behavior of the air-electrode has not yet been clarified.

In this study, LABs employing ILs consisting of Li-TFSA as the lithium salt, the $TFSA^-$ anion as the anion, and aliphatic cation species as the cation were prepared. The cyclic Py_{13}^+ cation and acyclic $DEME^+$ cation were selected as the aliphatic cations, and the effect of the electrolyte structure on the interfacial behavior of the air-electrode was investigated. As a comparison, the organic solvent-based electrolyte containing Li-TFSA as the lithium salt and LiBr (as a redox mediator, RM) mixed with $LiNO_3$ was employed.

2. Experimental Method

2.1 Preparation of electrolytes

By adding Li-TFSA (Kanto Chemical Co., 99.7 %) to G4 (Sigma-Aldrich, 99.9 %), Py_{13}-TFSA (Kanto Chemical Co., 99.9 %), and DEME-TFSA (Kanto Chemical Co., 99.9 %), 1 mol dm^{-3} Li-TFSA/G4 (hereafter denoted as the G4 system), Li-TFSA/Py_{13}-TFSA (hereafter denoted as the Py_{13} system), and Li-TFSA/DEME-TFSA (hereafter denoted as the DEME system) were prepared. As a pretreatment, Li-TFSA was ground in an agate mortar, then dried under reduced pressure (353 K, 1 h). All the ILs were used as received. $LiNO_3$ (Kanto Chemical Co., 99.9 %) and LiBr (Kanto Chemical Co., 96.0 %) as the RM were mixed at the molar ratio of 1 : 0.05. By adding the above mixed salt to G4, 1 mol dm^{-3} $LiNO_3$ + 0.05 mol dm^{-3} LiBr/G4 (hereafter denoted as the $LiNO_3$ system) was prepared. After the preparation, the electrolyte was obtained by stirring at 333 K and 300 rpm for 12 hours. All the electrolytes were prepared in a gas-circulating glove box (Miwa Seisakusho, DBO-1 NKP-1 U-2 Model) filled with pure Ar gas (Nikko Oxygen, high purity).

2.2 Evaluation of electrolyte properties

An SVM[10] 3001 (Anton Paar) was used to measure the density and viscosity of the electrolyte. CON 11 & CON 110 (OAKION) was used to measure the electrical conductivity. The physical properties were measured at 298 K under an Ar atmosphere.

2.3 Preparation of test cells

Using a carbon electrode for the air-electrode of the LABs and a Li foil (Honjo Chemical Co., thickness: 0.17 mm) for the negative electrode, a CR 2032 coin-type cell (Hosen Co., SUS 316 L) was fabricated. A type 2032 mesh case (Hosen Co., SUS 316 L, porosity: 51 %) was employed for the top cover of the air-electrode of the above cell. Ketjen black (KB, LION, ECP600JD) powder of carbon material and binder were stirred (R.T., 5 min) at the weight ratio of 90 : 10 (wt%), then the slurry was prepared using a dispersing medium. Polyvinylidene fluoride (Kureha Co., KF Polymer # 9130, 5 wt%) was used as the binder and *N*-methyl-2 pyrrolidone (Kanto Chemical Co., 99.5 %) used as the dispersing medium. The slurry was coated on carbon paper (CP, MOUBIC, Avcarb P50) as the current collector at a thickness of 10 µm, dried under reduced pressure at 353 K for 3 hours, then a disk with a diameter of 16 mm was prepared as the air-electrode. The Li foil and a piece of glass fiber filter paper (Whatman GF/A, CELGARD, thickness: 25 µm, porosity: 39 %, air permeability (gurley value): 620 seconds) as a separator disk were formed with a diameter of 16 mm. The air-electrode was placed on the lower lid, and 50 µL of electrolyte was dropwise added. The separator and the negative electrode were placed on it, the upper lid was then put on, and a caulking operation was carried out using a caulking device (Egaer-Corporation, KTE-20 S-D). All operations were carried out in a gas-circulating glove box filled with pure Ar gas.

2.4 Electrochemical measurement of LABs

To evaluate the electrochemical characteristics of the LABs, constant-current discharge-charge tests were performed. The cathodic reaction, in which Li^+ and O_2 react at the air-electrode to produce Li_2O_2, and the anodic reaction, in which Li_2O_2 decomposes to produce Li^+ and O_2, were defined as the discharge-charge reaction, respectively. Constant-current discharge-charge tests were performed on the fabricated coin cell using an automatic battery charging-discharging instrument (Hokuto Denko, HJR-1010mSM8), the fabricated coin cells were tested at a current density of 50 µA cm^{-2} in the voltage range of 2.0–4.3 V with an open circuit time of 5 min and a discharge capacity controlled at 200 mAh $(g\text{-carbon})^{-1}$. All the discharge-charge capacities were converted per amount of loaded carbon material.

A frequency response analyzer (Toyo Technica, 1255 B) was connected to an electrochemical measurement system (Toyo Technica, SI 1287) for the electrochemical impedance (EIS) measurements. Using the fabricated coin cells, measurements were made in the frequency range of 100 kHz–10 mHz with an amplitude voltage of ±10 mV. Impedance analysis software (Scribner Associate, Z-View, 32 ver. 2.4) was used for fitting the data. All the electrochemical measurements were performed at 298 K in dry air (natural convection).

3. Results and Discussion

3.1 Electrolyte properties

Table 1 shows the physical properties of various electrolytes at 298 K. The upper and lower row shows the measured values in this study and the literature values,[7,14–19] respectively. All the measured values were similar to those in the literature. The viscosity of the IL system was higher than that of the organic solvent system, which was comparable to previous results. In particular, the viscosity of the DEME system was higher than that of the Py_{13} system. This is because the distance from the cation center of the $DEME^+$ cation to the ether oxygen is long, and the cation loses its structural flexibility. This reduces the free volume of the cation and increases the viscosity.[20] On the other hand, the electrical conductivity of the Py_{13} system was almost the same as that of the organic solvent system, while that of the DEME system was lower.

3.2 Discharge-charge characteristics and cycling performance of the LABs using various electrolytes

Figure 2 shows the discharge-charge curves of LABs using various electrolytes at 298 K for (a) the 1st cycle and (b) the 50th cycle. The dotted line in the figure indicates the theoretical voltage of the LABs of 2.96 V.[21] The difference between the theoretical voltage and the charge voltage is defined as the charge overvoltage, and the difference between the theoretical voltage and the discharge voltage is defined as the discharge overvoltage, and their total is defined as the overvoltage of the LABs.[21–23] Figures S1 and S2 show the overvoltage of the 1st cycle and 50th cycle, respectively. In this study, the charge capacity of the DEME system did not reach 200 mAh $(g\text{-carbon})^{-1}$, therefore, the overvoltage was compared at the capacity of 100 mAh $(g\text{-carbon})^{-1}$.

Table 1. Density, viscosity, and electrical conductivity of various electrolytes at 298 K.

Electrolytes	Density $g\,cm^{-3}$	Viscosity mPa s	Electrical conductivity $mS\,cm^{-1}$
Li-TFSA/G4	0.94	10.4	1.18
	1.16[7]	$5 < x < 10$[14]	2.72[14]
$LiNO_3$ + LiBr/G4	1.05	14.3	1.84
	—	10.2[15]	1.5[15]
Li-TFSA/Py_{13}-TFSA	1.31	64.4	1.38
	1.37[16]	63[17]	1.40[17]
Li-TFSA/DEME-TFSA	1.34	239.4	0.68
	1.38[18]	<210[18]	0.61[19]

In Fig. 2a, the DEME system exhibited the charge capacity of ca. 127 mAh $(g\text{-carbon})^{-1}$, while the other systems exhibited almost 200 mAh $(g\text{-carbon})^{-1}$. The 1st discharge-charge efficiencies of the G4, $LiNO_3$, Py_{13}, and DEME systems were 99.9 %, 99.7 %, 99.4 %, and 64.5 %, respectively. In Fig. S1, the charge overvoltages of the Py_{13}, $LiNO_3$, G4, and DEME systems at the charge capacity of 100 mAh $(g\text{-carbon})^{-1}$ were 0.59 V, 0.76 V, 1.01 V, and 1.34 V, respectively, while the discharge overvoltages were 0.29 V, 0.39 V, 0.52 V, and 0.88 V, respectively, in the order of the Py_{13}, G4, $LiNO_3$, and DEME systems. Compared to the overvoltages of the organic solvent systems, the overvoltage of the DEME system was higher and that of the Py_{13} system was lower. The lower charge overvoltage of the $LiNO_3$ system compared to that of the G4 system is considered to be due to the presence of RM.[24] The charge overvoltage of the Py_{13} system was lower than that of the $LiNO_3$ system using the RM. The low electrical conductivity of the DEME system was considered to have increased the internal resistance of the cell, resulting in a high overvoltage. This would coincide with the results that the semicircle of the DEME system from the medium to low frequency region was larger than the Py_{13} system in the Nyquist plots of impedance spectra described later. This would be caused by the blockage of the O_2 diffusion path due to the residual discharge products and by-products to the air-electrode, which inhibits the supply of O_2 required for the electrode reaction. The discharge-charge characteristics of the LABs are affected by the formation[24] and deposition states[22] of the discharge products. In the ILs systems containing the $TFSA^-$ anions, it has been reported that the reductive decomposition of the $TFSA^-$ anions occurs and the formation of the $-SO_2CF_3$ species is dominating.[25] Therefore, in the Py_{13} and DEME systems, by-products including the $-SO_2CF_3$ species would be formed not only on the Li negative electrode surface, but also on the air-electrode during discharge, i.e., reductive decomposition. The discharge overvoltage of DEME system was more than 0.5 V higher than that of the Py_{13} system, so it is possible that many by-products were formed by the reductive decomposition of the $TFSA^-$ anion. Therefore, it is considered that the discharge-charge efficiency of the DEME system was low.

In Fig. 2b, the discharge capacities of the Py_{13} and $LiNO_3$ systems after 50 cycles were maintained at 200 mAh $(g\text{-carbon})^{-1}$, while those of the G4 and DEME systems did not reach 200 mAh $(g\text{-carbon})^{-1}$. The discharge-charge efficiencies of the DEME and $LiNO_3$ systems were 88.7 % and 84.7 %, respectively, while those of

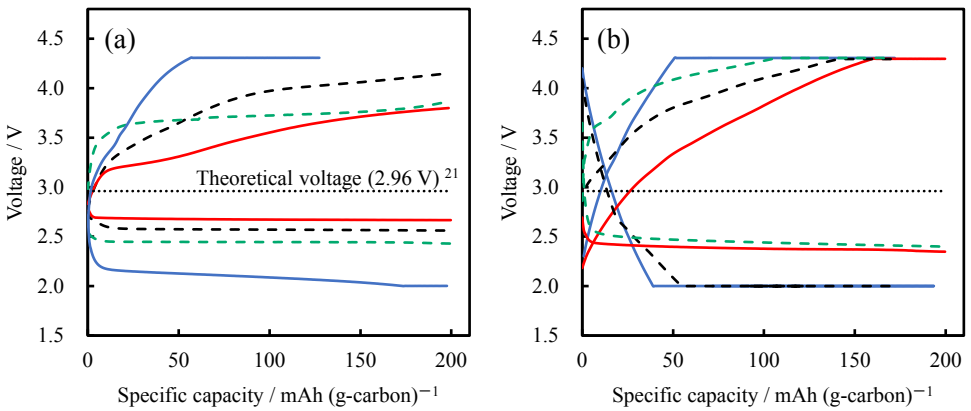

Figure 2. Discharge-charge curves for LABs with various electrolytes after (a) the 1st cycle (b) and the 50th cycle at 298 K; current density: 50 $\mu A\,cm^{-2}$; voltage range: 2.0–4.3 V; limit capacity: 200 mAh $(g\text{-carbon})^{-1}$; loading weight of KB: 0.5 $mg\,cm^{-2}$. The electrolytes are Li-TFSA/Py_{13}-TFSA (red solid line), Li-TFSA/DEME-TFSA (blue solid line), Li-TFSA/G4 (black dashed line), and $LiNO_3$ + LiBr/G4 (green dashed line).

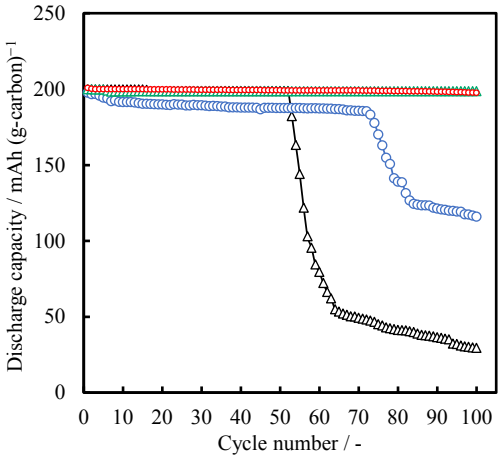

Figure 3. Dependence of cycling performance on the discharge capacities for LABs with various electrolytes at 298 K; current density: 50 μA cm^{-2}; voltage range: 2.0–4.3 V; limit capacity: 200 mAh (g-carbon)$^{-1}$; loading weight of KB: 0.5 mg cm^{-2}. The electrolytes are Li-TFSA/Py_{13}-TFSA (red open circle), Li-TFSA/DEME-TFSA (blue open circle), Li-TFSA/G4 (black open triangle), and $LiNO_3$ + LiBr/G4 (green open triangle).

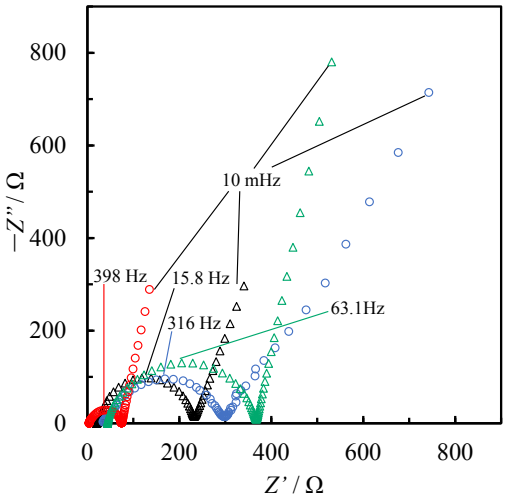

Figure 4. Nyquist plots of impedance spectra of LABs with various electrolytes after first charge at 298 K; frequency range: 100 kHz–10 mHz, AC amplitude: ±10 mV. The electrolytes are Li-TFSA/Py_{13}-TFSA (red open circle), Li-TFSA/DEME-TFSA (blue open circle), Li-TFSA/G4 (black open triangle), and $LiNO_3$ + LiBr/G4 (green open triangle).

the Py_{13} and G4 systems were 99.9 % and 98.8 %, respectively. The charge overvoltages for the Py_{13}, G4, $LiNO_3$, and DEME systems at the 50th cycle were 0.88 V, 1.14 V, 1.32 V, and 1.34 V, respectively. The discharge overvoltages were 0.59 V, 0.97 V, 0.52 V, and 0.96 V, respectively, and the overvoltages at the 50th cycle increased compared to the 1st cycle. This would be due to the reported discharge-charge reactions, which led to deposition of the discharge products on the KB surface of the air-electrode, resulting in clogging. In addition, the formation of by-products consumed the electrolyte, decreasing the electrical conductivity of the electrolyte and increasing the internal resistance of the cell.

Figure 3 shows the cycling performance of the discharge capacity for LABs with various electrolytes up to 100 cycles. While the discharge capacities of the G4 and DEME systems rapidly decreased from the 53rd and 74th cycles, respectively, both the Py_{13} and $LiNO_3$ systems maintained approximately 200 mAh (g-carbon)$^{-1}$ up to 100 cycles. The oxygen solubility of the Py_{13} system (1.31 mg L^{-1}) is lower than that of the G4 system (8.40 mg L^{-1}).[11] Furthermore, since the ILs containing pyrrolidinium cations are relatively stable to the O_2^- reaction intermediate,[26] it is considered that the decomposition of the Py_{13} system is relatively suppressed and the discharge-charge reactions were stable. As already described, it was shown that the cycling performance of the organic solvent system changed by charging the Li salts. On the other hand, in the IL system of Li-TFSA as the Li salt, the cycling performance varied depending on the type of the cation species, and the Py_{13} system revealed the best cycling performance.

To verify the effect of the type of cationic species in the ILs on the discharge-charge characteristics, the interfacial behavior of the LABs was analyzed using EIS. Figure 4 shows the Nyquist plots of impedance spectra of the LABs with various electrolytes at 298 K after the 1st charge cycle. For all the electrolytes, a capacitive semicircle was observed in the medium frequency region and a straight line around 45° in the low frequency region. In the two-electrode type cell, it has been reported that charge transfer occurs on the Li negative electrode surface and the air-electrode surface in the medium frequency region.[11] It is considered that the high to medium frequency region represents the negative electrode, the medium to low frequency region represents the interface resistance of the air-electrode, and the low frequency region represents the diffusion resistance of the air-electrode. The Py_{13} system has the lowest semicircle in the medium frequency region, indicating that the interface resistance after the 1st cycle charge was the lowest. On the other hand, although the interface resistance of the DEME system was lower than that of the $LiNO_3$ system, the diffusion resistance in the low frequency region was higher. This is correlated with the high viscosity of the DEME system, which would have slowed down the diffusion of Li^+ and O_2. Based on these results, a high agreement was observed in the interfacial resistance and the discharge-charge characteristics of the LABs in the ILs system.

4. Conclusion

LABs employing the amide-based ILs with the aliphatic cation species and $TFSA^-$ anion as the electrolyte were prepared and the electrochemical characteristics were evaluated, and the following results were obtained.

1) The overvoltage of the LABs employing the Py_{13} system was lower than those employing the DEME system and the organic solvent-based electrolyte.
2) Compared to the LABs employing the DEME and G4 systems as the electrolytes, the cycling performance of the Py_{13} system was almost the same as that of the $LiNO_3$ system, showing an excellent discharge capacity of 200 mAh (g-carbon)$^{-1}$ at the 100th cycle.
3) As a result of analyzing the interfacial behavior by EIS, the Py_{13} system showed the lowest interfacial resistance among the 4 types of electrolytes.

Based on these results, it has been clarified that employing the amide-based ILs containing the Py_{13}^+ cation with a relatively high electrical conductivity and low viscosity as the electrolyte results in a good cycling performance due to low overvoltage and interfacial resistance during the discharge-charge reaction. In the future, the discharge products deposited on the surface of the air-electrode will be analyzed and then the correlation with the discharge-charge characteristics will be discussed in more detail.

Acknowledgment

This work was supported in part by JSPS KAKENHI Grant Number JP21K05253.

CRediT Authorship Contribution Statement

Koichi Ui: Funding acquisition (Lead), Investigation (Lead), Project administration (Lead), Resources (Lead), Supervision (Lead), Writing – review & editing (Lead)
Sota Nakamura: Data curation (Lead), Formal analysis (Lead), Investigation (Equal), Writing – original draft (Lead)
Yushi Sato: Data curation (Equal), Formal analysis (Equal), Investigation (Equal)
Tatsuya Takeguchi: Funding acquisition (Supporting), Supervision (Supporting), Writing – review & editing (Supporting)
Masayuki Itagaki: Supervision (Supporting), Writing – review & editing (Supporting)

Data Availability Statement

The data that support the findings of this study are openly available under the terms of the designated Creative Commons License in J-STAGE Data listed in D1 of References.

Conflict of Interest

The authors declare no conflict of interest in the manuscript.

Funding

Japan Society for the Promotion of Science: JP21K05253

References

D1. K. Ui, S. Nakamura, Y. Sato, T. Takeguchi, and M. Itagaki, *J-STAGE Data*, https://doi.org/10.50892/data.electrochemistry.25132577, (2024).
1. A. C. Luntz and B. D. McCloskey, *Chem. Rev.*, **114**, 11721 (2014).
2. S. Matsuda, E. Yasukawa, T. Kameda, S. Kimura, S. Yamaguchi, Y. Kudo, and K. Uosaki, *Cell Rep. Phys. Sci.*, **2**, 100506 (2021).
3. M. Piana, J. Wandt, S. Meini, I. Buchberger, N. Tsiouvaras, and H. A. Gasteiger, *J. Electrochem. Soc.*, **161**, A1992 (2014).
4. J. M. Tarascon and M. Armand, *Nature*, **414**, 359 (2001).
5. R. Black, S. H. Oh, J. H. Lee, T. Yim, B. Adams, and L. F. Nazer, *J. Am. Chem. Soc.*, **134**, 2902 (2012).
6. K. U. Schwenke, S. Meini, X. Wu, H. A. Gasteiger, and M. Piana, *Phys. Chem. Chem. Phys.*, **15**, 11830 (2013).
7. M. Saito, T. Fujinami, S. Yamada, T. Ishikawa, H. Otsuka, K. Ito, and Y. Kudo, *J. Electrochem. Soc.*, **164**, A2872 (2017).
8. K. Nishioka, M. Tanaka, H. Fujimoto, T. Amaya, S. Ogoshi, M. Tobisu, and S. Nakanishi, *Angew. Chem., Int. Ed.*, **134**, e202112769 (2022).
9. Z. J. Chen, T. Xue, and J. M. Lee, *RSC Adv.*, **2**, 10564 (2012).
10. G. Wang, S. Shen, S. Fang, D. Luo, L. Yang, and S. Hirano, *RSC Adv.*, **6**, 71489 (2016).
11. Y. Li, Z. Zhang, D. Duan, Y. Sun, G. Wei, X. Hao, S. Liu, Y. Han, and W. Meng, *J. Power Sources*, **329**, 207 (2016).
12. H. Nakamoto, Y. Suzuki, T. Shiotsuki, F. Mizuno, S. Higashi, K. Takechi, T. Asaoka, H. Nishikoori, and H. Iba, *J. Power Sources*, **243**, 19 (2013).
13. U. Ulissi, G. A. Elia, S. Jeong, J. Reiter, N. Tsiouvaras, S. Passerini, and J. Hassoun, *Chem. Eur. J.*, **24**, 3178 (2018).
14. J. Chen, C. Chen, T. Huang, and A. Yu, *ACS Omega*, **4**, 20708 (2019).
15. M. Ono and S. Matsuda, *J. Phys. Chem. C*, **127**, 6117 (2023).
16. H. Sakaebe, H. Matsumoto, and K. Tatsumi, *J. Power Sources*, **146**, 693 (2005).
17. D. R. MacFarlane, P. Meakin, J. Sun, N. Animi, and M. Forsyth, *J. Phys. Chem. B*, **103**, 4164 (1999).
18. S. D. Talian, M. Bešter-Rogac, and R. Dominko, *Electrochim. Acta*, **252**, 147 (2017).
19. K. Tsunashima, F. Yonekawa, and M. Sugiya, *Chem. Lett.*, **37**, 314 (2008).
20. A. R. Neale, P. Li, J. Jacquemin, P. Goodrich, S. C. Ball, R. G. Compton, and C. Hardacre, *Phys. Chem. Chem. Phys.*, **18**, 11251 (2016).
21. P. Xu, C. Chen, J. Zhu, P. Zhao, and M. Wang, *J. Electroanal. Chem.*, **842**, 98 (2019).
22. Y. Liu, L. Wang, L. Cao, C. Shang, Z. Wang, H. Wang, L. He, J. Yang, H. Cheng, J. Li, and Z. Lu, *Mater. Chem. Front.*, **1**, 2495 (2017).
23. Z. Wu, Y. Tian, H. Chen, L. Wang, S. Qian, T. Wu, S. Zhang, and J. Lu, *Chem. Soc. Rev.*, **51**, 8045 (2022).
24. X. Xin, K. Ito, and Y. Kudo, *ACS Appl. Mater. Interfaces*, **9**, 25976 (2017).
25. S. Xiong, K. Xie, E. Blomberg, P. Jacobsson, and A. Matic, *J. Power Sources*, **252**, 150 (2014).
26. F. Mizuno, K. Takechi, S. Higashi, T. Shiga, T. Shiotsuki, N. Takazawa, Y. Sakurabayashi, S. Okazaki, I. Nitta, T. Kodama, H. Nakamoto, H. Nishikoori, S. Nakanishi, Y. Kotani, and H. Iba, *J. Power Sources*, **228**, 47 (2013).